INTERNATIONAL JOURNAL OF CLIMATOLOGY
Int. J. Climatol. (2016)
Published online in Wiley Online Library
(wileyonlinelibrary.com) DOI: 10.1002/joc.4729

RMetS
Royal Meteorological Society

Trajectory patterns of the annual cycle of the heat centre of the Indo-Pacific warm pool

Haixia Shan,[a,b,c,d,e,f] Yuping Guan,[b]* Jianping Huang[g] and Changming Dong[a,h]*

[a] *Oceanic Modeling and Observation Laboratory, College of Marine Science, Nanjing University of Information Science &Technology, China*
[b] *State Key Laboratory of Tropical Oceanography, South China Sea Institute of Oceanology, Chinese Academy of Sciences, Guangzhou, China*
[c] *Jiangsu Engineering Technology Research Center of Marine Environment Detection, Nanjing University of Information Science & Technology, Nanjing, China*
[d] *Key Laboratory of Meteorological Disaster of Ministry of Education, Nanjing University of Information Science & Technology, Nanjing, China*
[e] *Joint International Research Laboratory of Climate and Environment Change, Nanjing University of Information Science & Technology, Nanjing, China*
[f] *Collaborative Innovation Center on Forecast and Evaluation of Meteorological Disasters, Nanjing University of Information Science & Technology, Nanjing, China*
[g] *Key Laboratory for Semi-Arid Climate Change of the Ministry of Education, College of Atmospheric Science, Lanzhou University, China*
[h] *Department of Atmospheric and Oceanic Sciences, University of California, Los Angeles, CA, USA*

ABSTRACT: The modulated annual cycle (MAC) of the Indo-Pacific warm pool (IPWP) heat centre location is investigated using the empirical mode decomposition–ensemble empirical mode decomposition method. The MAC and its interannual variability mainly affect the zonal and vertical locations of the heat centre; in fall and winter of El Niño years, the heat centre moves eastward from its normal location, with very little change in its meridional position. Four patterns of the heat centre trajectory in the IPWP are identified using the self-organizing map algorithm. Patterns 1 and 3 are both similar to a saddle, but pattern 1 is more winding. The shapes of patterns 2 and 4 are similar, but tilt in different directions: pattern 2 tilts southwest whereas pattern 4 tilts west. Of all the four patterns, the persistence of pattern 2 is generally relatively high. The trajectory of the heat centre develops in the sequence of patterns: 1-2-4-3-1. Pattern 1 (pattern 4) is related to the cold (warm) phase of the El Niño–Southern Oscillation (ENSO), while pattern 2 (pattern 3) corresponds to the negative (positive) phase of Indian Ocean dipole (IOD). The sequence of patterns in the trajectory of the heat centre in the IPWP is related to the IOD–ENSO interactions on a biennial timescale.

KEY WORDS heat centre; Indo-Pacific warm pool; self-organizing map; ensemble empirical mode decomposition

Received 6 May 2015; Revised 13 February 2016; Accepted 7 March 2016

1. Introduction

The Indo-Pacific warm pool (IPWP) is the most extensive and warmest water mass in the world's oceans. As such, it is a major region of atmospheric convection and a major source of heat for driving global atmospheric circulation (Gadgil *et al.*, 1984). Warm waters supply the atmosphere with water vapour and heat and result in heavy rainfall in excess of 2–3 m per year (Chen *et al.*, 2004). Because the saturation vapour pressure is an exponential function of sea surface temperature (SST), also known as the Clausius–Clapeyron relationship, a small change in SST results in a dramatic change in atmospheric convection. Changes in the warm pool can alter atmospheric divergent flow locally and affect the Walker and Hadley circulations, causing a globally intense climate response (Sardeshmukh and Hoskins, 1988; Neale and Slingo, 2003; Enfield *et al.*, 2006). The ocean circulation in the IPWP and surrounding ocean is complex and changeable. There are a number of equatorial currents and western boundary currents that play an important part in the marine zonal and meridional heat and mass transport, and in the exchange of Pacific waters between the Northern and Southern Hemispheres.

In this article, the IPWP is characterized by sea temperatures higher than 28 °C (Yan *et al.*, 1997; Chen and Fang, 2005; Clement *et al.*, 2005; Zhang *et al.*, 2007). This is based on the fact that the depth of the 28 °C isotherm makes the IPWP an enclosed water mass, and that the onset of atmospheric deep convection occurs when temperatures exceed 28 °C (Fu *et al.*, 1994). During the last few years, warm pool properties such as the surface centroid (Ho *et al.*, 1995; Yan *et al.*, 1997, 2002; Fang, 2005), the eastern edge (Picaut *et al.*, 1997; McPhaden, 1999) and the volume or area features (Meinen and McPhaden, 2000, 2001; Yan *et al.*, 2002; Zhou *et al.*, 2004) have been investigated. The solar irradiance variability, El Niño–Southern Oscillation (ENSO) events and global warming possibly

* Correspondence to: Y. Guan, South China Sea Institute of Oceanology, Chinese Academy of Sciences, Guangzhou 510301, China. E-mail: guan@scsio.ac.cn or C.Dong, Oceanic Modeling and Observation Laboratory, College of Marine Science, Nanjing University of Information Science & Technology, Nanjing 210044, China. E-mail: cmdong@gmail.com

© 2016 Royal Meteorological Society

causes the SST and the size of the warm pool to fluctuate (Yan *et al.*, 1992). The movement of warm pool and convective activity affect Walker and Hadley circulations, causing a global climate response (Wang and Enfield, 2001; Enfield *et al.*, 2006). The continuous expansion of the size of the IPWP since the 1980s represents an increase in the total heat energy available to heat the tropospheric air, which lifts the tropical cold-point tropopause height and leads to the observed long-term cooling trend of the tropical cold-point tropopause temperature (Xie *et al.*, 2014a, 2014b).

Philander (1990), Ho *et al.* (1995) and Yan *et al.* (1997) computed and analysed the movements of the warm pool and they found that the centroid of the warm pool is an indicator when studying the interactions between the ocean and atmosphere and the El Niño events because the locations of the centroid in these El Niño periods are controlled by the overall shape and position of the warm pool, which in turn are controlled by anomalous equatorial currents driven by winds. In earlier work, some authors (Ho *et al.*, 1995; Yan *et al.*, 1997, 2002; Fang, 2005) defined the warm pool centroid as the surface 'geometric centre'. This definition only considers the shape of the outer boundary of the warm pool (i.e. the 28 °C isotherm), while its inner thermal structure is totally neglected. This would not be a problem if the SST gradients within the warm pool were all concentric. However, the SST pattern of the warm pool is considerably asymmetric about its warm core (Chen and Fang, 2005). A new scheme for determining the warm pool centroid which takes into account the thermal structure of the surface water was proposed by Chen and Fang (2005). Compared to previous work, their definition resulted in a significant improvement in the precise tracking of the warm pool trajectory. In particular, Chen and Fang (2005) found that the two definitions make a significant difference: mean biases of 5.59° in the zonal direction and 0.46° in the meridional direction, with maximum biases reaching 11.62° and 2.67°, respectively. The new scheme for warm pool centroid estimation is expected to help explain the shift in convective activity in the equatorial Pacific, and hence, improve our understanding of ENSO-related phenomena in this region. In this study, we make use of measurements as a function of all three space dimensions to define the 'thermal centroid' (hereafter, referred to as the heat centre) of the IPWP. Ho *et al.* (1995), Yan *et al.* (1997) and Fang (2005) found that the movement of the centroid of western Pacific warm pool (WPWP) traces an ellipse-like trajectory and moves counterclockwise in most of the years.

The mean annual cycle of a climate variable is conventionally defined as the climatological monthly/daily mean of the data for a given period, which is assumed repetitive from year to year. Wu *et al.* (2008) proposed an alternative reference frame for climate anomalies, the modulated annual cycle (MAC) using the empirical mode decomposition (EMD) and ensemble empirical mode decomposition (EEMD) method that allows the annual cycle to change from year to year. The effectiveness of the EMD–EEMD method has been recently documented in many geophysical applications (Huang and Wu, 2008; Wu *et al.*, 2008; Qian *et al.*, 2009, 2010, 2011a, 2011b, 2011c; Ruzmaikin and Feynman, 2009; Wu and Huang, 2009; Franzke, 2010; Breaker and Ruzmaikin, 2011; Franzke and Woollings, 2011; Qian and Zhou, 2014; Shan *et al.*, 2014). In particular, the ability of EEMD and the advantage of using it to extract the annual cycle component (which has strong amplitude–frequency modulation) from a climate variable have been validated using synthetic data, monthly SST data and daily surface air temperature records (Wu *et al.*, 2008; Qian *et al.*, 2011a).

The studies (Vinayachandran and Shetye, 1991; Fang, 2005) referred to the annual cycle of warm pool using the traditional definition of annual cycle. The previous studies (Yan *et al.*, 1997) have defined the heat centre as the surface centroid and studied its trajectory on the surface. To our knowledge, there is no previous study that investigates the patterns of the trajectory of the heat centre in three-dimensional space. The purpose of our study is to investigate the amplitude and phase changes of the annual cycle of the heat centre in the IPWP. The patterns of trajectory of MAC of heat centre in the IPWP are classified using the self-organizing map (SOM) technique (Kohonen, 1982). The warm pool characteristics for different patterns are also presented. In addition, the evolution of the patterns and what is related to them are discussed in detail.

2. Data and methods

2.1. Data

The ocean dataset used in this study is obtained from the Simple Ocean Data Assimilation (SODA) 2.2.4 (Giese and Ray, 2011), which is available from 1871 to 2008. The ocean model of SODA is based on Parallel Ocean Program (POP) with an average $0.25° \times 0.4° \times 40$-level resolution. Horizontal mixing is biharmonic and vertical mixing uses the K-profile parameterization. Rivers are also included with climatological seasonal discharge. The surface boundary conditions such as surface wind, solar radiation, specific humidity, cloud cover, 2 m air temperature, precipitation are provided from a new atmospheric dataset (Compo *et al.*, 2011) designated as Twentieth Century Reanalysis version 2 (20CRv2). Observations include virtually all available hydrographic profile data, ocean station data, moored temperature and salinity time series, surface temperature and salinity observations of various types, and nighttime infrared satellite SST data. The output is in monthly averaged form, mapped onto a uniform $0.5° \times 0.5° \times 40$-level grid.

2.2. Methods

This study uses the same methodology as Shan *et al.* (2014), therefore, we briefly repeat it here. It is assumed that the IPWP is a relatively homogeneous water mass and that the movement of the IPWP heat centre represents the evolution of the shape and position of the IPWP itself. The zonal, meridional and vertical locations of the IPWP heat centre are calculated in the region enclosed by the 28 °C

© 2016 Royal Meteorological Society

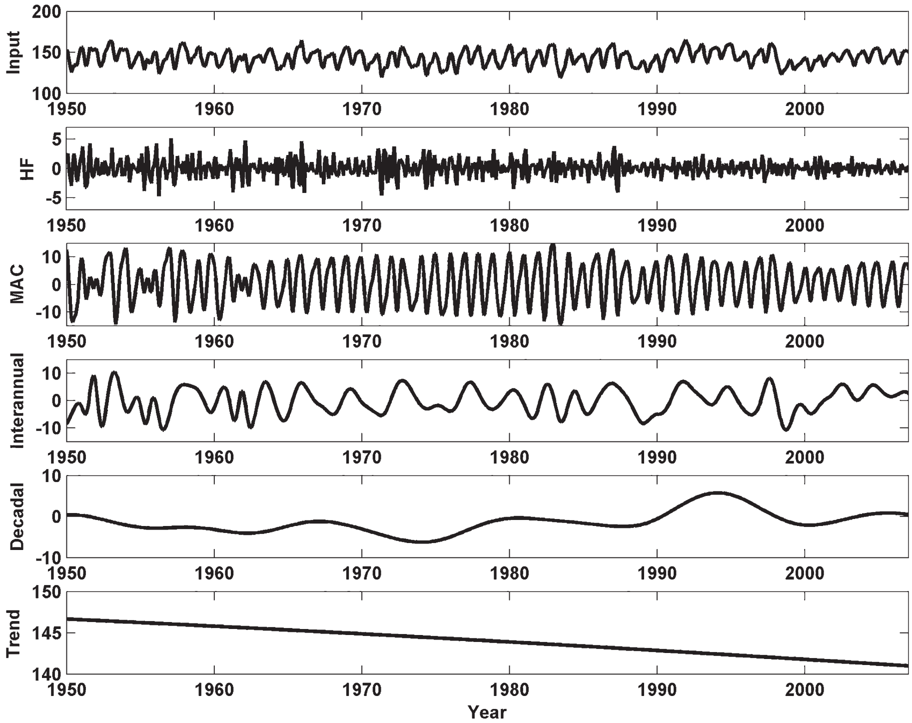

Figure 1. Decomposition and reconstruction of the IPWP zonal heat centre location from January 1950 to December 2007. 'Input' stands for the raw monthly data.

isotherm (between 30°S–30°N and 30°E–120°W). The heat centre $\overline{X}_i$ ($i=1, 2, 3$) are defined as follows (Chen and Fang, 2005):

$$\overline{X}_i = \frac{\sum_{j=1}^{n} w_j X_{ij}}{\sum_{j=1}^{n} w_j}, \quad i = 1,2,3 \tag{1}$$

$$w_j = \frac{T_j - T_{\min}}{T_{\max} - T_{\min}} \tag{2}$$

where the subscripts 1, 2, and 3 denote, respectively, the zonal, meridional and vertical directions, n is the number of grid points in the three-dimensional warm pool, X_{ij} is the sea water location at point j, T_j is the temperature of sea water at point j and w_j is a normalized weighting function. $T_{\max}$ and $T_{\min}$ are the maximum and minimum sea temperature. Hence, $\overline{X}_i$ ($i=1, 2, 3$) indicates the longitude, latitude and depth of the heat centre of warm pool, respectively.

We use an adaptive and temporally local data analysis tool – the EMD and EEMD method (Huang and Wu, 2008; Wu and Huang, 2009) – to extract the annual cycle, hereafter, referred to as the amplitude–frequency MAC (Wu *et al.*, 2008). Because linear trends are sensitive to the analysis period or small changes at the beginning and/or end of the selected data domain, we examine the nonlinear and adaptive trend of a climate variable. Climate variables are defined as an intrinsically fitted monotonic function or a function in which there can be at most one extremum within a given data span (Wu *et al.*, 2007).

This classification is based on the SOM (Kohonen, 1982), which is an unsupervised artificial neural network that reduces a high-dimensional dataset into a low-dimensional one that summarizes the key aspects of the larger dataset into a set of patterns, and it is also known as Kohonen map. Details of the approach are given by Cassano *et al.* (2006). The SOM has been shown to be more powerful than conventional methods (e.g. the empirical orthogonal functions) for the purpose of extracting consistent features (Reusch *et al.*, 2005; Liu *et al.*, 2006), and has been successfully applied in climate research (Morioka *et al.*, 2010; Chattopadhyay *et al.*, 2013). The SOM algorithm produces a one-dimensional set of patterns of the heat centre trajectory. After testing several different sizes, the final shape of the chosen Kohonen map for our study is a 2×2 matrix of heat centre patterns that can cover most of the aspects of trajectory features, also ensuring that each pattern can provide robust statistics for the properties of the warm pool. We use the batch training algorithm, which is more computationally efficient than the sequential algorithm (Vesanto *et al.*, 1999, 2000). The neighbourhood function chosen is 'ep' which gives the most accurate patterns (Liu *et al.*, 2006).

3. Results

3.1. The basic features of the IPWP heat centre

We first reconstruct the IPWP heat centre location into five major time-scale components (the zonal locations of the heat centre is shown in Figure 1) using the method introduced by Wu *et al.* (2008). They are (Figure 1) the

© 2016 Royal Meteorological Society

Table 1. The contribution of the different time-scale components of heat centre to the total variances.

Index	HF	MAC	Interannual	Decadal	Trend
Zonal of heat centre	3.91	40.03	28.32	18.93	8.79
Meridional of heat centre	3.48	93.72	1.28	1.42	0.06
Vertical of heat centre	6.74	24.76	51.01	11.71	5.76

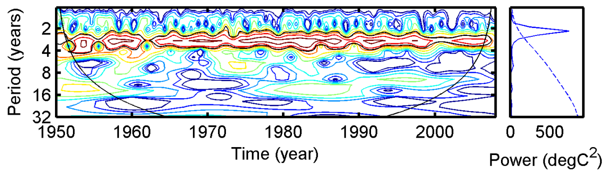

Figure 2. A wavelet analysis for the MAC of heat centre in zonal direction. Wavelet power spectra and corresponding global wavelet spectra, where dashed lines indicate a significance level at $p < 0.05$.

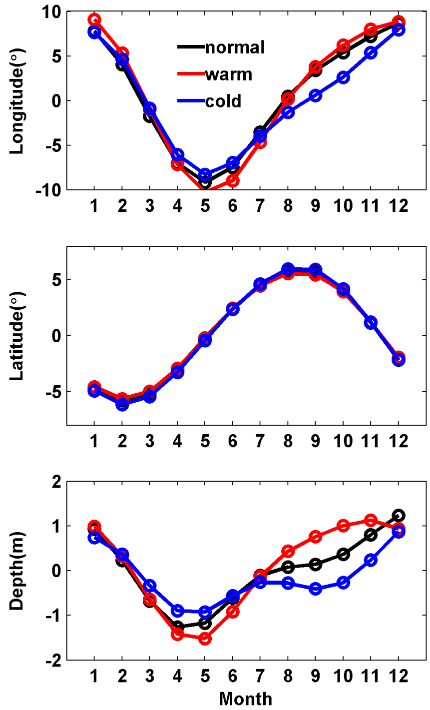

Figure 3. Composites of the MAC of heat centre in zonal, meridional and vertical directions in IPWP for the period 1950–2007 during El Niño (warm), La Niña (cold) and normal years.

high-frequency (HF) component representing intra-annual variability, the MAC component representing the annual cycle, the interannual time-scale component representing interannual variation within a period of 2–7 years, the decadal component and the trend component. Because the data prior to 1950 is of poor quality, and to eliminate the minor influence of end effects on our results, the last few years of all the decomposed results are excluded, leaving the period 1950–2007 to be analysed. The contributions of the different components to the total variance of the heat centre are also calculated (see Table 1). It can be seen from Table 1 that the MAC and interannual variability are more important for zonal and vertical locations of heat centre. In particular as to the meridional location of heat centre, the MAC component can contribute 93.72% for the total variance. Figure 2 illustrates the wavelet power spectra and corresponding global wavelet spectra of the MAC of the heat centre in zonal direction, using Morlet wavelet analysis (Torrence and Compo, 1998). It is evident that MAC contains variability of a quasi-1-year period throughout the data span.

The different features of MAC of IPWP heat centre during El Niño and La Niña event years are displayed in Figure 3. The classification of the El Niño years and La Niña follows the method of Qian *et al.* (2011c). Table 2 shows the ENSO events from 1950 to 2007. Although we use different datasets, most of them are consistent with the results of Qian *et al.* (2011c). As to the meridional component of the heat centre, the MAC component accounts for more than 90% of the total variance. The difference of the meridional component of the heat centre in different years is very small, only that in El Niño years it is a little smaller in summer and bigger in winter. That is to say the change of the meridional component of the heat centre is confined to a smaller extent in the meridional direction. On the other hand, the zonal location of the heat centre from April to August lies to the west, while from July to December it lies to the east of its location in normal years. As to the heat centre's vertical location in El Niño years, from March to August it is at much shallower depths, while from September to February it is at much deeper depths. The El Niño exhibits significant seasonal coherence, with SST anomalies emerging in boreal summer, peaking in early winter and decaying in the following spring (Wang and Fiedler, 2006; Xie *et al.*, 2009). When an El Niño event takes place, there is an anomalous eastward advection of warm water because of anomalous westerly wind, which can result in the heat centre moving eastward than in the normal years, the relaxation of trade wind also leads to the flattering of the thermocline, which can generate an anomalous poleward geostrophic transport (Bosc and Delcroix, 2008). The meridional location of the heat centre is to the north on average. Thus, the heat centre lies to the north of its normal location during the mature phase of an El Niño event.

Amplitude change of the MAC component of heat centre of the IPWP together with their secular trends are illustrated in Figure 4. The amplitude of the MAC component of the zonal heat centre increases before 1980s and decreases after that. The meridional component of heat centre has no obvious trend. The amplitude of the vertical component of the IPWP heat centre decreases before 1960, increases before 1980, and then, decreases thereafter. The timing of the transition from a cold to a warm phase for the MAC is calculated as the date when the MAC intersects zero (estimated using linear interpolation) (Figure 5). Because there are many years that the vertical component of the heat centre has no intersections with zero

© 2016 Royal Meteorological Society

Table 2. Classification of ENSO events from 1950 to 2007. Weak (W): peak strength reaches 0.5–1 °C, moderate (M): 1–1.5 °C and strong (S): >1.5 °C.

El Niño			La Niña		
Peak	Strength	Duration	Peak	Strength	Duration
1951/10	M (1.1174)	1951/5–1952/3	1950/6	W (−0.7943)	1950/1–1950/10
1953/7	W (0.8417)	1953/3–1953/11	1955/11	M (−1.1010)	1954/7–1956/8
1957/11	M (1.0722)	1957/4–1958/5	1962/6	W (−0.7041)	1962/1–1962/10
1963/8	W (0.7453)	1963/6–1963/11	1964/8	W (−0.8924)	1964/5–1964/12
1965/9	M (1.3372)	1965/4–1966/3	1967/10	W (−0.8553)	1966/11–1968/3
1969/12	M (1.1610)	1968/12–1970/3	1970/11	S (−1.8863)	1970/6–1971/3
1972/10	S (2.0661)	1972/4–1974–4	1973/11	M (−1.0425)	1973/8–1974/5
1976/11	M (1.0540)	1976/6–1977/6	1975/9	W (−0.8216)	1975/4–1975/12
1983/1	S (1.7726)	1982/6–1983/7	1981/9	W (−0.8737)	1981/5–1982/1
1987/5	S (1.5828)	1986/8–1987/12	1984/5	W (−0.9624)	1983/12–1986/1
1992/1	W (0.9265)	1991/7/1992/7	1988/10	M (−1.4079)	1988/4–1989/6
1997/11	S (2.8432)	1997/4–1998/7	1996/9	M (−1.2955)	1995/4–1997/1
2002/9	W (0.6817)	2002/6–2002/12	1999/4	M (−1.3524)	1998/10–2000/4
2004/9	W (0.5336)	2004/6–2004/12	2007/11	W (−0.8694)	2007/7–2008/5
2006/9	W (0.7390)	2006/7–2006/12			

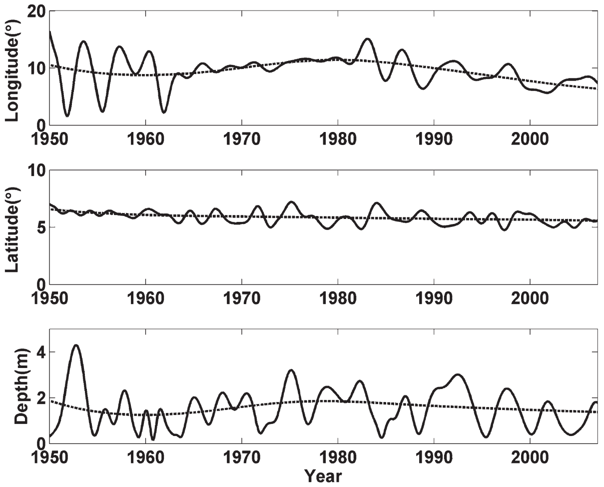

Figure 4. Amplitude change of the MAC component of heat centre in zonal, meridional and vertical directions in IPWP together with their secular trends (dashed lines) fitted by EEMD.

(from a positive phase to a negative phase), only the zonal and meridional components of the heat centre trajectory are displayed in Figure 5. As to the zonal component of the heat centre trajectory, the date when the IPWP moves from east to west comes earlier and earlier during the periods 1950–1965 and 1975–2007, and much later between 1965 and 1975. When it comes to the meridional component, the date when the IPWP moves from south to north is much later before 1960 and much earlier during the period 1960–1970, after which there is no obvious change.

3.2. Trajectory patterns of IPWP

The patterns of the trajectories for the MAC component of the IPWP heat centre produced by the SOM algorithm, and their frequencies of occurrence are shown in Figure 6. Pattern 2 appears most frequently (31.1%), although all patterns are approximately equally distributed. Patterns 1 and 3 are like a saddle, with pattern 1 being much more

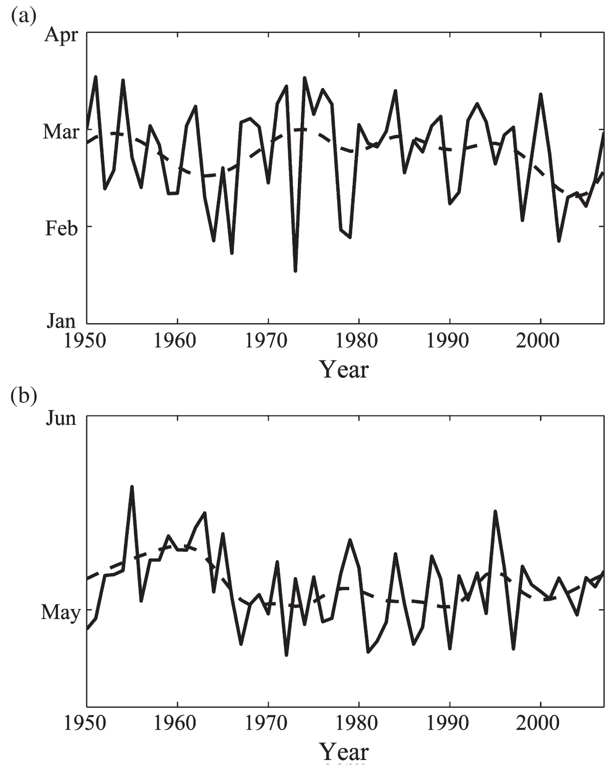

Figure 5. Phase (timing of the annual cycle transition from the cold to the warm phase) change of the MAC component of heat centre in zonal (a), meridional (b) directions, together with their secular trends (dashed lines) fitted by EEMD.

winding. The shapes of patterns 2 and 4 are similar, but they tilt in different directions. Pattern 2 tilts towards the southwest and pattern 4 tilts to the west.

Figure 7 shows the details of the likelihood of persistence of each pattern and the transition to the other patterns. The first value shown as a percentage inside the rectangle is the likelihood of persistence, i.e. the first one for the following year looks much like that for the present year

© 2016 Royal Meteorological Society

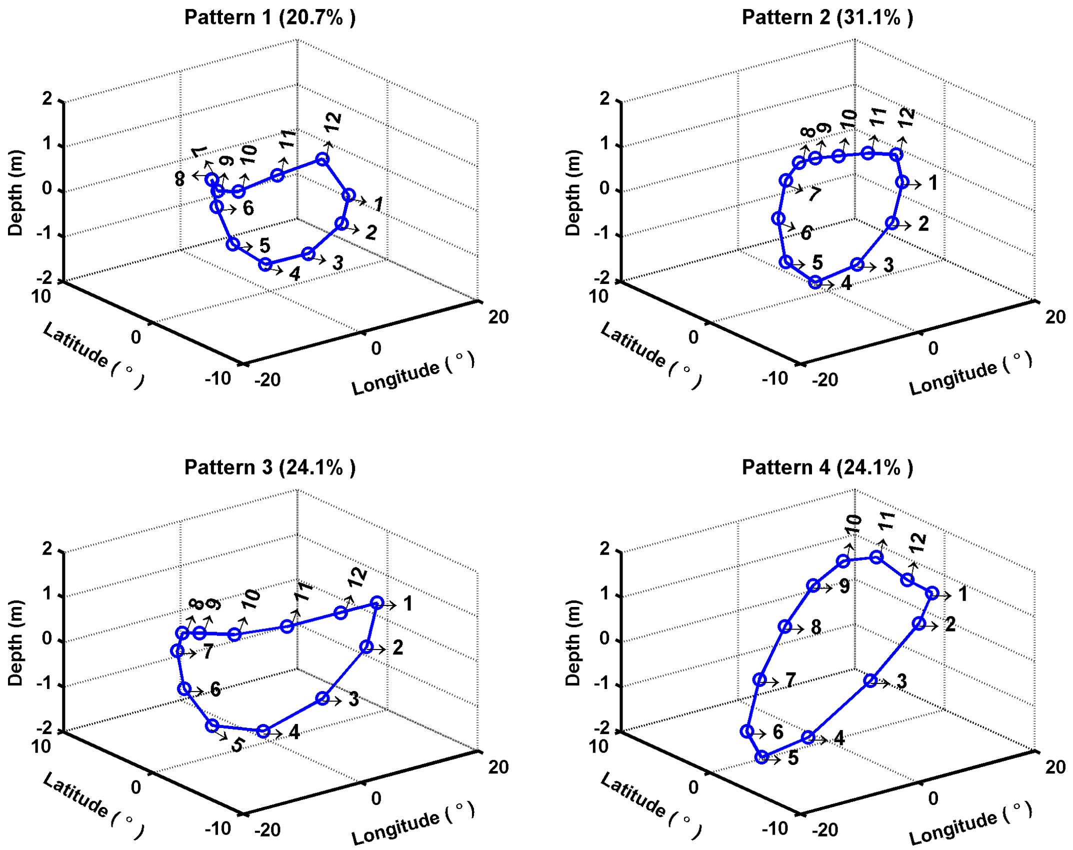

Figure 6. Patterns of trajectory of MAC of heat centre and their occurrence frequency (%) using SOM.

and thus, also matches best with the same pattern. The second value adjacent to the arrows is transition likelihood, shows the most likely change to occur when persistence does not apply. The following year is sufficiently different from the present year that it matches better with a different pattern. For example, if pattern 1 is the best match for a year, there is a 16.67% chance that it will also be the best match for the next year, but a probability of 66.66% of changing to pattern 2 and a 16.67% chance of changing to pattern 3. Of all the four patterns, the persistence of pattern 2 is generally relatively high. If the percentages are based on the number of events left after persistence has been removed, i.e. if three out of ten events involved persistence, then the transition percentage shown is based on the remaining seven events. In this case, in pattern 1 there is an 80% chance of changing to pattern 2 (and a 20% chance of changing to one of the remaining patterns). Pattern 2 has a 54.54% likelihood of changing to pattern 4, and pattern 4 has a 49.99% probability of changing to pattern 3. In addition, pattern 3 has a 40% probability of transforming to patterns 1 and 4. Figure 7 suggests that the heat centre trajectory develops along the sequence of patterns: 1-2-4-3 and then back to 1.

To further show the mean state of the IPWP associated with each pattern of the heat centre trajectory, Figure 8 shows the vertical structure of the ocean temperature differences of the four patterns compared with the mean temperature for 1950–2007 averaged between 2.5°S and 2.5°N. The reason for choosing the mean temperature

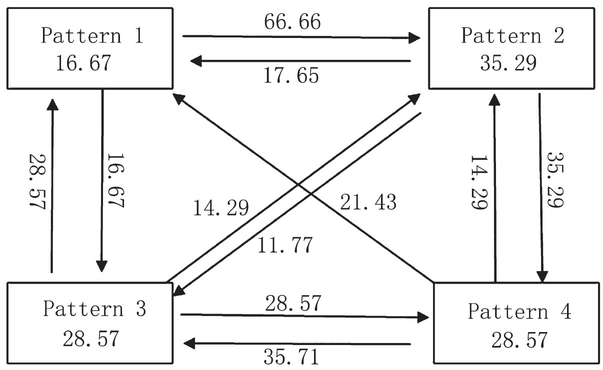

Figure 7. The persistence and transition likelihood (in %) of the four patterns of MAC of heat centre in IPWP. Persistence is indicated by percentages shown within each pattern. Percentages near arrows indicate likelihood of transition to the other patterns.

averaged between 2.5°S and 2.5°N is that the IPWP has an approximate zonal dimension near the equator (Wang and Metha, 2008). The difference between patterns 1 (shown in Figure 8(a)) and the climatology is that the equatorial eastern Pacific is much colder, especially for depths above 200 m, and it is much warmer in the western Pacific. The difference with climatology represented in pattern 2 (Figure 8(b)) shows that it is much warmer in the western Pacific and the Indian Ocean, whereas in pattern 3 (Figure 8(c)) it is colder in the Indian Ocean above 150 m, and the cooling in the eastern and middle Pacific is much

© 2016 Royal Meteorological Society

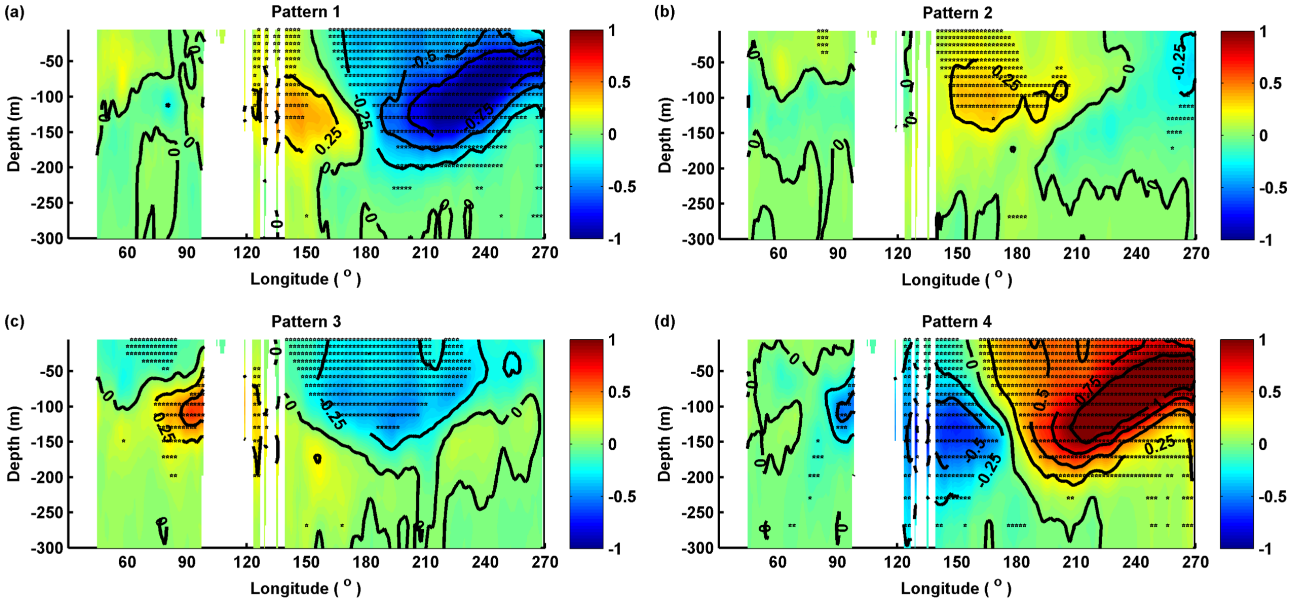

Figure 8. The ocean temperature differences compared with the mean value (1950–2007) over 2.5°S–2.5°N in four patterns. Dark shadings indicate temperature differences at the 5% significance level.

stronger. When it comes to pattern 4 (Figure 8(d)), however, the difference with climatology is much warmer in the eastern Pacific and much colder in the western Pacific.

The IPWP has its maximum meridional extension near 150°E. Figure 9 shows the vertical-meridional cross section for ocean temperature along 150°E. In pattern 1 (shown in Figure 9(a)), it is much warmer in the region 10°S–10°N, especially for depths between 50 and 200 m. The state of sea temperature in pattern 4 (Figure 9(d)) is opposite to that in pattern 1. As to pattern 3 (Figure 9(c)), the remarkable warming is mainly found in the region 0°–10°N. However, in pattern 2 (Figure 9(b)), notable warming is located between 10°S and 0°N. Furthermore, the remarkable warming in both patterns 2 and 3 is between 100 and 200 m, while in pattern 2 (pattern 3) the ocean is warmer (colder) above 100 m between latitudes 10°S and 20°N.

Figure 10 displays the different shapes of the IPWP for the four patterns. The eastern extension of the IPWP shows remarkable difference in the four patterns (Figure 10(a)). In pattern 1, the eastern extension of IPWP is the smallest but the northern expanding is the largest. In addition, the north branch is the deepest and the southern extension of the south branch of the IPWP is also the largest. The condition in pattern 4 is contrary to that in pattern 1. In pattern 2, the vertical extension is much deeper, especially the south branch of IPWP. In pattern 3, the vertical extension in the Indian Ocean is the shallowest, and the west boundary extends eastward. Furthermore, the south branch is to the south compared with pattern 2.

The shallow meridional overturning circulation, which is also known as the subtropical cell (STC) (Liu, 1994; McCreary and Lu, 1994), controls the transport of mass, heat and salt between the equator and the subtropics, and plays an important part in oceanic climate variability. The STC is closed by upwelling at the equator, a poleward Ekman transport at the surface, subduction in the subtropics and an equatorward flow within the thermocline. A vertical cross section of mean meridional velocity difference at 150°–155°E relative to the mean condition (1950–2007) associated with the four patterns is shown in Figure 11. The STC in both the hemispheres strengthens in pattern 1 (displayed in Figure 11(a)), but it weakens in pattern 4 (Figure 11(d)). Stronger STCs may lead to a stronger subduction and warming of the ocean temperature under the surface. In pattern 1, for example, a stronger STC warms the warm pool, which favours the heat centre moving to the north. The changes in pattern 4 are the opposite of this situation. In pattern 3 (Figure 11(c)), the Northern Hemisphere STC is weak, cooling the warm pool in the Northern Hemisphere and causing the heat centre to move to the south. In pattern 2 (Figure 11(b)), a stronger Northern Hemisphere STC warms the warm pool in the Northern Hemisphere.

4. Discussion

Ho *et al.* (1995) and Yan *et al.* (1997) showed that the zonal and meridional displacements of the WPWP are controlled by El Niño events and the annual solar irradiance cycle, respectively. Because the total volume of the WPWP is on an average three times that in the Indian Ocean warm pool (Vinayachandran and Shetye, 1991), the IPWP heat centre is mainly controlled by the WPWP. The trajectory of the heat centre MAC during El Niño and La Niña years is shown in Figure 12. It can be seen that pattern 1 is like that during La Niña years, and pattern 4 resembles the situation in El Niño years. From the cluster time series (Figure 13), we see that the years when pattern 1 occurs are nearly consistent with La Niña years (Table 2).

© 2016 Royal Meteorological Society

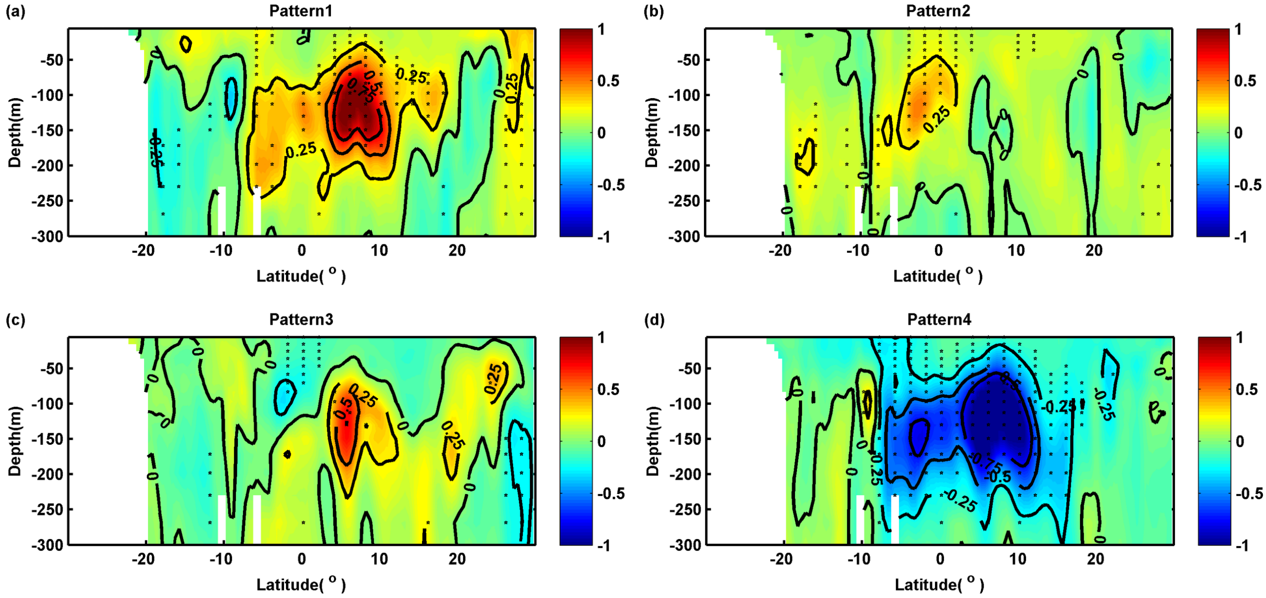

Figure 9. As in Figure 8, but for a latitude–depth cross section at 150°E.

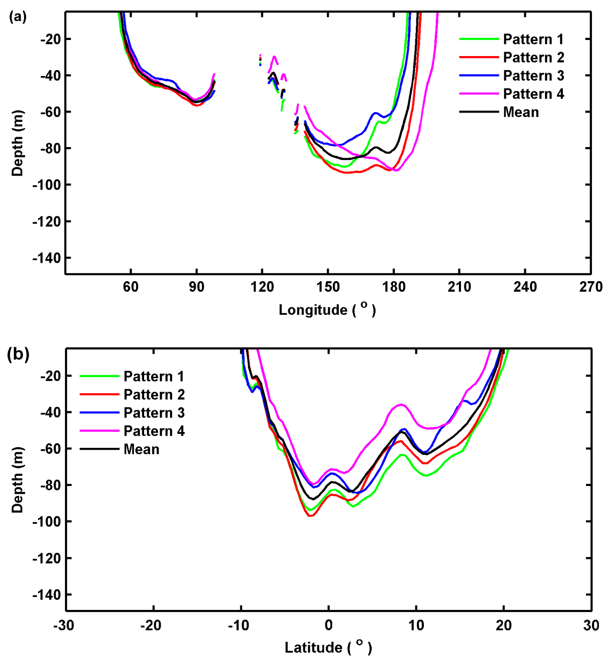

Figure 10. The comparison of the shape of IPWP in the four patterns and climatology (a) is for that over 2.5°S–2.5°N, and (b) is that in a latitude–depth cross section at 150°E.

Likewise, the years when pattern 4 occurs nearly matches the El Niño years (Table 2). Yan *et al.* (1999) also indicated that the WPWP centroid moves clockwise with a northeast-southwest orientation during the year of El Niño onset, which is similar to our results.

As mentioned above, in pattern 1, it is much colder in the equatorial eastern Pacific and much warmer in the western Pacific. During La Niña years, anomalous easterly winds pile up warm water in the west, causing the heat centre of IPWP move to the west, and expand in the vertical dimension. In pattern 4, it is much warmer in the eastern Pacific and much colder in the western Pacific. The sea temperature distribution in pattern 4 is opposite to that in pattern 1, which corresponds to El Niño years when anomalous westerly winds permit warm water to advect eastward.

Figure 14 shows the 5 m sea temperature differences compared with the mean value (1950–2007) for patterns 2 and 3. For pattern 3 (pattern 2), there is a positive (negative) SST anomaly in the western part of the Indian Ocean and a negative (positive) anomaly in the eastern part. This is similar to the Indian Ocean dipole (IOD) (Saji *et al.*, 1999; Webster *et al.*, 1999), with pattern 3 (pattern 2) corresponding to the positive (negative) phase of the IOD. In pattern 2, the western Pacific and the Indian Ocean is much warmer, which expands the Indian Ocean warm pool. While in pattern 3, the west boundary of IPWP is to the east of Indian Ocean.

In the previous section, it was shown that the trajectory of the heat centre evolves in the pattern sequence 1-2-4-3-1. An El Niño event tends to favour easterly wind anomalies over the equatorial Indian Ocean, which can trigger a positive IOD and Indian Ocean basin-wide warming (Annamalai *et al.*, 2003; Luo *et al.*, 2010). Schott *et al.* (2009) has reviewed mechanisms on how ENSO exerts its influence on the circulation and SST of the Indian Ocean through an atmospheric bridge and triggers the IOD. In response to wind variations in the Pacific promoted by both IOD events (Izumo *et al.*, 2010) and Indian Ocean basin-wide warming (Annamalai *et al.*, 2005; Kug *et al.*, 2006; Ohba and Ueda, 2007), a positive IOD in fall and basin-wide warming in winter both promote a transition towards a La Niña event in the following year. A negative IOD can force equatorial Pacific easterly wind anomalies and drive positive SST anomalies in the central Pacific through zonal advection of the warm pool eastern edge. The SST anomalies may be enhanced by the Bjerknes

© 2016 Royal Meteorological Society

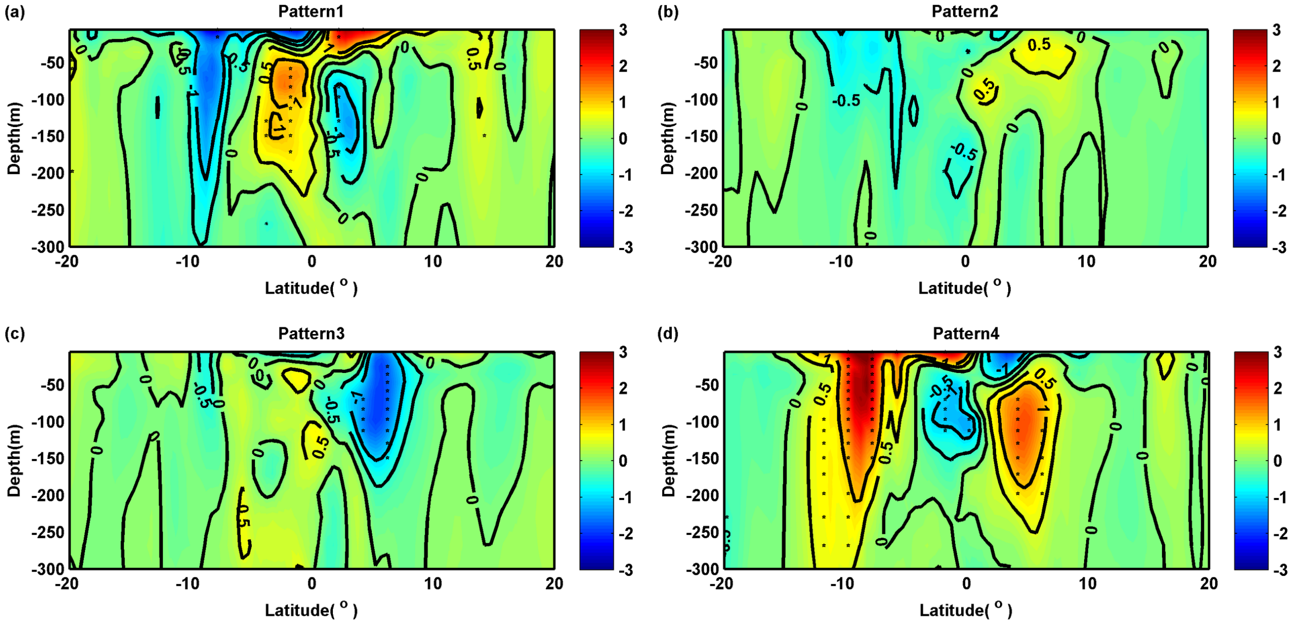

Figure 11. As in Figure 8, but for the meridional velocity difference at 150°–155°E.

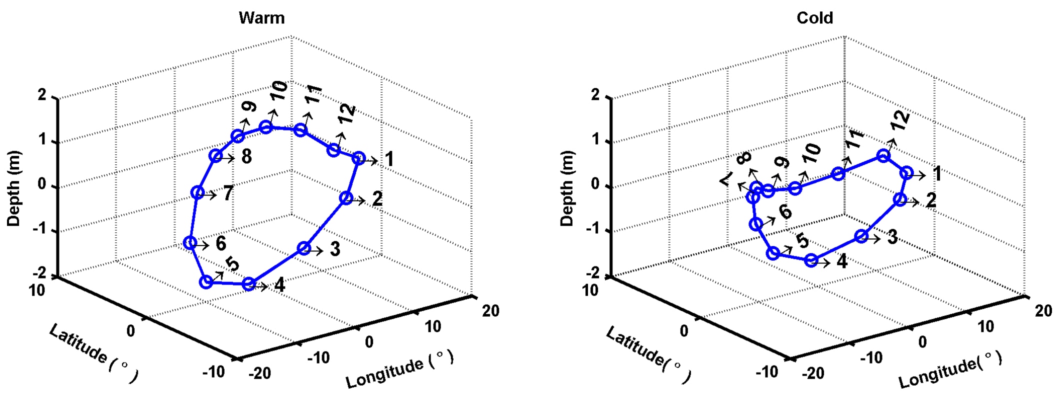

Figure 12. Trajectory of mean MAC of heat centre for IPWP during El Niño (warm), La Niña (cold) years.

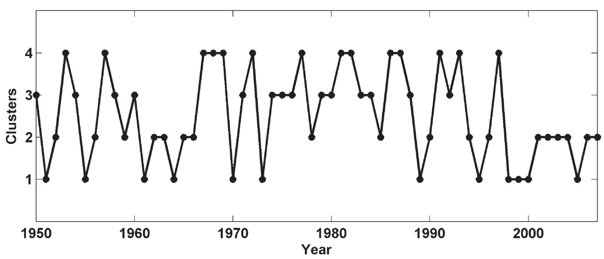

Figure 13. The clusters time series of MAC of heat centre in IPWP.

feedback and develop into an El Niño event (Izumo *et al.*, 2014). The transition of the IPWP heat centre trajectory is related to the IOD–ENSO interactions on a biennial timescale (Izumo *et al.*, 2014).

5. Summary

The MAC of the IPWP heat centre (in longitudinal, latitudinal and vertical directions) is first obtained based on the EMD–EEMD method. The basic features of the heat centre MAC are investigated. We found that both the MAC and interannual variability are important for the zonal and vertical locations of the heat centre, but MAC dominates for the meridional location. The different features of the heat centre MAC during El Niño and La Niña years were discussed. In normal years from April to August, the zonal component of the IPWP heat centre is located in the west, while during July to December it moves to the east. In El Niño years from March to August, the vertical component is at shallower depths, while from September to February it is much deeper. El Niño is in a mature phase in winter and warm water is advected to the eastern part of the Pacific because of the anomalous westerly winds, which can cause the heat centre moving to the east. The relaxation of trade wind leads to the flattering of the thermocline across the equatorial ocean, which can generate an anomalous poleward geostrophic transport. As a result, the heat centre lies to the north in El Niño years. Amplitude and phase changes (from a cold phase to a warm phase) of the heat centre MAC were also studied.

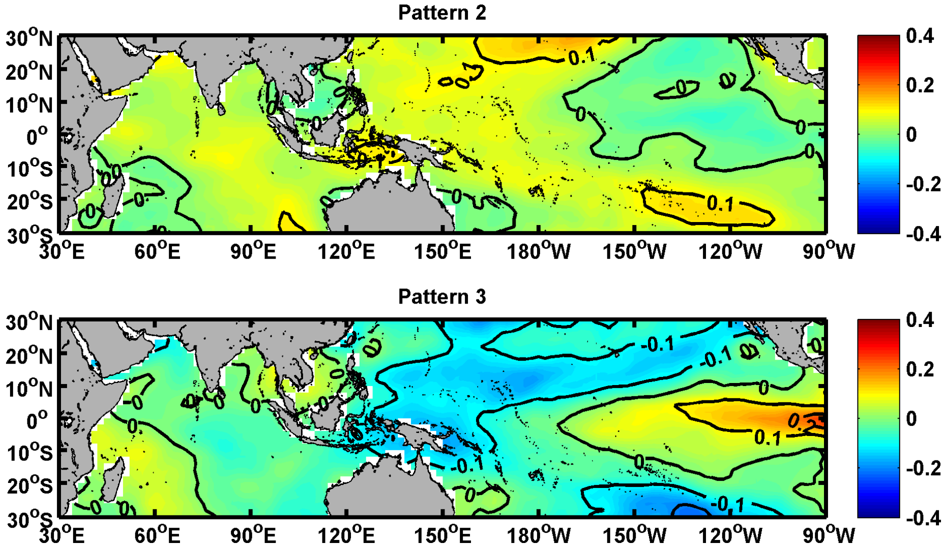

Figure 14. The 5 m temperature differences compared with the mean value (1950–2007) in patterns 2 and 3

The IPWP heat centre MAC trajectory patterns were classified using the SOM algorithm. Patterns 1 and 3 are like a saddle, with pattern 1 being more winding. The shapes of patterns 2 and 4 are similar, but they tilt in different directions. Pattern 2 tilts towards the southwest and pattern 4 tilts to the west. Of all four patterns, the persistence of pattern 2 is relatively longer. The heat centre trajectory develops in the pattern sequence: 1-2-4-3-1. Pattern 1 (pattern 4) is related to the cold (warm) phase of ENSO, while pattern 2 (pattern 3) corresponds to the negative (positive) phase of IOD. The transitions of the IPWP heat centre trajectory are related to IOD–ENSO interactions on a biennial timescale.

Acknowledgements

This work was supported by Natural Science Foundation of Jiangsu Province (No. BK20150912),China Postdoctoral Science Foundation funded project (2015M581834), State Key Laboratory of Tropical Oceanography, South China Sea Institute of Oceanology, Chinese Academy of Sciences (No. LTO1506) and the Priority Academic Program Development of Jiangsu Higher Education Institutions (PAPD). C.D. appreciates the supports from NSFC (41476022, 41490643, 91128204), Startup Foundation for Introducing Talent of Nanjing University of Information Science and Technology (2013r121, 2014r072), Program for Innovation Research and Entrepreneurship team in Jiangsu Province and National Program on Global Change and Air-Sea Interaction (No. GASI-03-IPOVAI-05).We would also like to thank the University of East Anglia for surface air temperature data and the University of Maryland and Texas A&M University for providing the SODA data. We also thank Dr Greg King from CSIC, Spain, for helping in proofreading the manuscript. We appreciate two anonymous reviewers for their constructive comments.

References

Annamalai H, Murtugudde R, Potemra J, Xie S-P, Liu P, Wang B. 2003. Coupled dynamics over the Indian Ocean: Spring initiation of the zonal mode. *Deep-Sea Res. II: Top Stud. Oceanogr.* **50**: 2305–2330, doi: 10.1016/S0967-0645(03)00058-4.

Annamalai H, Xie S-P, McCreary J-P, Murtugudde R. 2005. Impact of Indian Ocean sea surface temperature on developing El Niño. *J. Clim.* **18**: 302–319, doi: 10.1175/JCLI-3268.1.

Bosc C, Delcroix T. 2008. Observed equatorial Rossby waves and ENSO-related warm water volume changes in the equatorial Pacific Ocean. *J. Geophys. Res.* **113**: C06003, doi: 10.1029/2007JC004613.

Breaker LC, Ruzmaikin A. 2011. The 154-year record of sea level at San Francisco: extracting the long-term trend, recent changes, and other tidbits. *Clim. Dyn.* **36**: 545–559, doi: 10.1007/s00382-010-0865-4.

Cassano JJ, Uotila P, Lynch A. 2006. Changes in synoptic weather patterns in the polar regions in the twentieth and twenty-first centuries, Part 1: Arctic. *Int. J. Climatol.* **26**: 1027–1049.

Chattopadhyay R, Vintzileos A, Zhang C. 2013. A description of the Madden–Julian oscillation based on a self-organizing map. *J. Clim.* **26**: 1716–1732.

Chen G, Fang LX. 2005. Improved scheme for determining the thermal centroid of the oceanic warm pool using sea surface temperature data. *J. Oceanogr.* **61**: 295–299.

Chen G, Fang C, Zhang C, Chen Y. 2004. Observing the coupling effect between warm pool and "rain pool" in the Pacific Ocean. *Remote Sens. Environ.* **91**: 153–159, doi: 10.1016/j.rse.2004.02.010.

Clement AC, Seager R, Murtugudde R. 2005. Why are there tropical warm pools? *J. Clim.* **18**(24): 5294–5311.

Compo GP, Whitaker JS, Sardeshmukh PD, Matsui N, Allan RJ, Yin X, Gleason BE, Vose RS Jr, Rutledge G, Bessemoulin P, Brönnimann S, Brunet M, Crouthamel RI, Grant AN, Groisman PY, Jones PD, Kruk MC, Kruger AC, Marshall GJ, Maugeri M, Mok HY, Nordli Ø, Ross TF, Trigo RM, Wang XL, Woodruff SD, Worley SJ. 2011. The twentieth century reanalysis project. *Q. J. R. Meteorol. Soc.* **137**: 1–28, doi: 10.1002/qj.776.

Enfield DB, Lee SK, Wang C. 2006. How are large western hemisphere warm pools formed? *Prog. Oceanogr.* **70**: 346–365.

Fang MQ. 2005. Movements of the Western Pacific Warm Pool centroid and their relationship to sea surface temperature changes in Niño regions. *J. Ocean Univ. China* **4**(2): 189–192.

Franzke C. 2010. Long-range dependence and climate noise characteristics of Antarctic temperature data. *J. Clim.* **23**: 6074–6081.

Franzke C, Woollings T. 2011. On the persistence and predictability properties of North Atlantic climate variability. *J. Clim.* **24**: 466–472.

Fu R, Del Genio AD, Rossow WB. 1994. Influence of ocean surface conditions on atmospheric vertical thermodynamic structure and deep convection. *J. Clim.* **7**: 1092–1108, doi: 10.1175/1520-0442(1994)007<1092:IOOSCO>2.0.CO;2.

Gadgil S, Joseph PV, Joshi NV. 1984. Ocean–atmosphere coupling over the monsoon region. *Nature* **312**: 141–143.

© 2016 Royal Meteorological Society

Giese BS, Ray S. 2011. El Niño variability in simple ocean data assimilation (SODA), 1871–2008. *J. Geophys. Res.* **116**: C02024, doi: 10.1029/2010JC006695.

Ho C-R, Yan X-H, Zheng Q. 1995. Satellite observations of upper-layer variabilities in the western Pacific warm pool. *Bull. Am. Meteorol. Soc.* **76**: 669–679.

Huang NE, Wu Z. 2008. A review on Hilbert-Huang transform: method and its applications to geophysical studies. *Rev. Geophys.* **46**: RG2006, doi: 10.1029/2007RG000228.

Izumo T, Vialard J, Lengaigne M, de Boyer Montegut C, Behera SK, Luo J-J, Cravatte S, Masson S, Yamagata T. 2010. Influence of the state of the Indian Ocean dipole on the following year's El Nino. *Nat. Geosci.* **3**: 168–172, doi: 10.1038/ngeo760.

Izumo T, Lengaigne M, Vialard J, Yamagata T, Madec G. 2014. Influence of Indian Ocean dipole and Pacific recharge on following year's El Niño: interdecadal robustness. *Clim. Dyn.* **42**: 291–310, doi: 10.1007/s00382-012-1628-1.

Kohonen T. 1982. Self-organized information of topologically correct features maps. *Biol. Cybern.* **43**: 59–69.

Kug J-S, Li T, An S-I, Kang I-S, Luo J-J, Masson S, Yamagata T. 2006. Role of the ENSO–Indian Ocean coupling on ENSO variability in a coupled GCM. *Geophys. Res. Lett.* **33**: L09710, doi: 10.1029/2005GL024916.

Liu Z. 1994. A simple model of the mass exchange between the subtropical and tropical ocean. *J. Phys. Oceanogr.* **24**: 1153–1165.

Liu Y, Weisberg RH, Moors CNK. 2006. Performance evaluation of the self-organizing map for feature extraction. *J. Geophys. Res.* **111**: C05018, doi: 10.1029/2005JC003117.

Luo J-J, Zhang R, Behera S, Masumoto Y, Jin F-F, Lukas R, Yamagata T. 2010. Interaction between El Niño and extreme Indian Ocean dipole. *J. Clim.* **23**: 726–742.

McCreary J, Lu P. 1994. Interaction between the subtropical and equatorial ocean circulation: the subtropical cell. *J. Phys. Oceanogr.* **24**: 466–497.

McPhaden MJ. 1999. Genesis and evolution of the 1997–98 El Niño. *Science* **283**: 950–954.

Meinen CS, McPhaden MJ. 2000. Observations of warm water volume changes in the equatorial Pacific and their relationship to El Niño and La Niña. *J. Clim.* **13**: 3551–3559.

Meinen CS, McPhaden MJ. 2001. Interannual variability in warm water volume transports in the equatorial Pacific during 1993–1999. *J. Phys. Oceanogr.* **31**: 1324–1345.

Morioka Y, Tozuka T, Yamagata T. 2010. Climate variability in the southern Indian Ocean as revealed by self-organizing maps. *Clim. Dyn.* **35**: 1075–1088.

Neale R, Slingo J. 2003. The maritime continent and its role in the global climate: a GCM study. *J. Clim.* **16**: 834–848.

Ohba M, Ueda H. 2007. An impact of SST anomalies in the Indian Ocean in acceleration of the El Niño to La Niña transition. *J. Meteorol. Soc. Jpn.* **85**: 335–348.

Philander SGH. 1990. *El Niño, La Niña, Southern Oscillation*. Academic Press: San Diego, CA, 293 pp.

Picaut J, Masia F, du Penhoat Y. 1997. An advective reflective conceptual model for the oscillatory nature of the ENSO. *Science* **277**: 633–636.

Qian C, Zhou T. 2014. Multidecadal variability of North China aridity and its relationship to PDO during 1900–2010. *J. Clim.* **27**: 1210–1222, doi: 10.1175/JCLI-D-13-00235.1.

Qian C, Fu C, Wu Z, Yan Z. 2009. On the secular change of spring onset at Stockholm. *Geophys. Res. Lett.* **36**: L12706, doi: 10.1029/2009GL038617.

Qian C, Wu Z, Fu C, Zhou T. 2010. On multi-timescale variability of temperature in China in modulated annual cycle reference frame. *Adv. Atmos. Sci.* **27**: 1169–1182, doi: 10.1007/s00376-009-9121-4.

Qian C, Fu C, Wu Z. 2011a. Changes in the amplitude of the temperature annual cycle in China and their implication for climate change research. *J. Clim.* **24**: 5292–5302.

Qian C, Fu CB, Wu Z, Yan ZW. 2011b. The role of changes in the annual cycle in earlier onset of climatic spring in northern China. *Adv. Atmos. Sci.* **28**(2): 284–296.

Qian C, Wu Z, Fu C, Wang D. 2011c. On changing El Niño: a view from time-varying annual cycle, interannual variability and mean state. *J. Clim.* **24**(24): 6486–6500.

Reusch DB, Alley RB, Hewitson BC. 2005. Relative performance of self-organizing maps and principal component analysis in pattern extraction from synthetic climatological data. *Polar Geogr.* **29**: 188–212.

Ruzmaikin A, Feynman J. 2009. Search for climate trends in satellite data. *Adv. Adapt. Data Anal.* **1**: 667–679.

Saji NH, Goswami BN, Vinayachandran PN, Yamagata T. 1999. A dipole mode in the tropical Indian Ocean. *Nature* **401**: 360–363.

Sardeshmukh PD, Hoskins BJ. 1988. The generation of global rotational flow by steady idealized tropical divergence. *J. Atmos. Sci.* **45**: 1228–1251.

Schott FA, Xie SP, McCreary JP. 2009. Indian Ocean circulation and climate variability. *Rev. Geophys.* **47**: RG1002, doi: 10.1029/2007RG000245.

Shan HX, Guan YP, Huang JP. 2014. Surface air temperature patterns on a decadal scale in China using self-organizing map and their relationship to Indo-Pacific warm pool. *Int. J. Climatol.* **34**: 3752–3765.

Torrence C, Compo GP. 1998. A practical guide to wavelet analysis. *Bull. Am. Meteorol. Soc.* **79**: 61–78.

Vesanto J, Himberg J, Alhoniemi E, Parhankangas J. 1999. Selforganizing map in Matlab: The SOM Toolbox. *Proceedings of the Matlab DSP Conference*: Espoo, Finland, pp. 34–40.

Vesanto J, Himberg J, Alhoniemi E, Parhankangas J. 2000. SOM toolbox for Matlab 5. Report No. A57, Helsinki University of Technology, Helsinki.

Vinayachandran PN, Shetye SR. 1991. The warm pool in the Indian Ocean. *Proc. Indian Acad. Sci.* **100**: 165–175.

Wang C, Enfield DB. 2001. The tropical Western Hemisphere warm pool. *Geophys Res Lett.* **28**: 1635–1638.

Wang C, Fiedler PC. 2006. ENSO variability and the eastern tropical Pacific: a review. *Prog. Oceanogr.* **69**: 239–266.

Wang H, Metha M. 2008. Decadal variability of the Indo-Pacific warm pool and its association with atmospheric and oceanic variability in the NCEP-NCAR and SODA reanalyses. *J. Clim.* **21**: 5545–5565, doi: 10.1175/2008JCLI2049.1.

Webster PJ, Moore AM, Loschnigg JP, Leben RR. 1999. Coupled ocean–atmosphere dynamics in the Indian Ocean during 1997–98. *Nature* **401**: 356–360.

Wu Z, Huang NE. 2009. Ensemble empirical mode decomposition: a noise-assisted data analysis method. *Adv. Adapt. Data Anal.* **1**: 1–41.

Wu Z, Huang NE, Long SR, Peng C-K. 2007. On the trend, detrending, and variability of nonlinear and nonstationary time series. *Proc. Natl. Acad. Sci.* **104**: 14889–14894.

Wu Z, Schneider EK, Kirtman BP, Sarachik ES, Huang NE, Tucker CJ. 2008. The modulated annual cycle: an alternative reference frame for climate anomalies. *Clim. Dyn.* **31**: 823–841.

Xie S-P, Hu K, Hafner J, Tokinaga H, Du Y, Huang G, Sampe T. 2009. Indian Ocean capacitor effect on Indo–western Pacific climate during the summer following El Niño. *J. Clim.* **22**: 730–747.

Xie F, Li JP, Tian WS, Li YJ, Feng J. 2014a. Indo-Pacific warm pool area expansion, modoki activity, and tropical cold-point tropopause temperature variations. *Sci. Rep.* **4**: 4552.

Xie F, Li JP, Tian WS, Zhang JK. 2014b. The relative impacts of El Niño Modoki, Canonical El Niño, and QBO on tropical ozone changes since the 1980s. *Environ. Res. Lett.* **9**: 064020.

Yan X-H, Ho C-R, Zheng Q, Klemas V. 1992. Temperature and size variability of the western Pacific warm pool. *Science* **258**: 1643–1645.

Yan X-H, He Y, Liu WT, Zheng Q, Ho C-R. 1997. Centroid motion of the western Pacific warm pool during three recent El Niño-Southern Oscillation events. *J. Phys.Oceanogr.* **27**: 837–845.

Yan X-H, He Y, Susanto RD, Liu WT. 1999. Multisensor studies on El Nino-Southern Oscillations and variabilities in equatorial Pacific. *J. Adv. Mar. Sci. Techn. Soc.* **4**(2): 289–301.

Yan X-H, Zhou YH, Pan JY, Zheng DW, Fang MQ, Liao XH, He MX, Liu WT, Ding XL. 2002. Pacific warm pool excitation, earth rotation and El Niño southern oscillations. *Geophys. Res. Lett.* **29**: 2301–2304.

Zhang QL, Qi QH, Hou YJ, Xu JP, Weng XC, Chen MH. 2007. Zonal displacement of western Pacific warm pool and zonal wind anomaly over the Pacific Ocean. *Chin. J. Oceanol. Limnol.* **25**(3): 277–285.

Zhou YH, Yan XH, Ding XL, Liao XH, Zheng DW, Pan JY, Fang MQ, He MX, Liu WT. 2004. Excitation of non-atmospheric polar motion by the migration of the Pacific Warm Pool. *J. Geod.* **78**: 109–113.

© 2016 Royal Meteorological Society